ACS APPLIED MATERIALS & INTERFACES

Research Article

www.acsami.org

Acidic Amorphous Silica Prepared from Iron Oxide of Bacterial Origin

Hideki Hashimoto,[†] Atsushi Itadani,[†] Takayuki Kudoh,[†] Yasushige Kuroda,[†] Masaharu Seno,[†] Yoshihiro Kusano,[‡] Yasunori Ikeda,[§] Makoto Nakanishi,[†] Tatsuo Fujii,[†] and Jun Takada*[,†,⊥]

[†]Graduate School of Natural Science and Technology, Okayama University, Okayama 700-8530, Japan

[‡]Department of Fine and Applied Arts, Kurashiki University of Science and the Arts, Kurashiki, Okayama, 712-8505, Japan

[§]Research Institute for Production Development, Sakyo-ku, Kyoto 606-0805, Japan

[⊥]JST, CREST, Okayama 700-8530, Japan

ABSTRACT: Microporous and mesoporous silica derived from biogenous iron oxide is an attractive catalyst for various organic reactions. Biogenous iron oxide contains structural silicon, and amorphous silica remains after iron oxide is dissolved in concentrated hydrochloric acid. The amorphous silica containing slight amounts of iron (Si/Fe = ~150) is composed of ~6-nm-diameter granular particles. The amorphous silica has a large surface area of 540 m^2/g with micropores (1.4 nm) and mesopores (<3 nm). By using pyridine vapor as a probe molecule to evaluate the active sites in the amorphous silica, it was found that this material has strong Brønsted and Lewis acid sites. When the catalytic performance of this material was evaluated for reactions including the ring opening of epoxides and Friedel–Crafts-type alkylations, which are known to be catalyzed by acid catalysts, this material showed yields higher than those obtained with common silica materials.

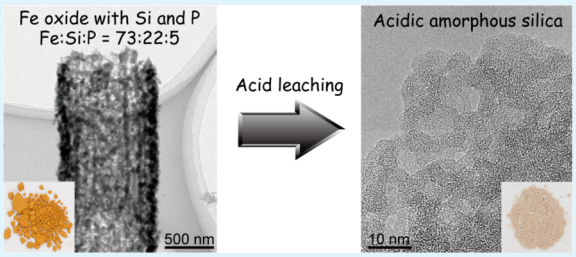

KEYWORDS: *amorphous silica, Brønsted acid, Lewis acid, acid catalysts, iron-oxidizing bacteria, biogenous iron oxide*

INTRODUCTION

Silicon-containing oxide materials such as synthetic and natural zeolites (SiO_2/Al_2O_3) have been industrially used as catalysts, adsorbents, and ion-exchange materials and are known to have very strong Brønsted and Lewis acid sites. They are practically applied as solid acid catalysts in various chemical reactions such as cracking reactions and isomerization and alkylation processes.[1] The acidity of zeolites is due to the hydroxyl protons in the Si···(OH)···Al framework (Brønsted acid) and extra-framework aluminum species or framework defects (Lewis acid).[1]

Generally, pure silica is known to be neutral or very slightly acidic. However, recently developed mesoporous amorphous silica materials (e.g., FSM-16 and MCM-41)[2−4] have been shown to have relatively strong acid sites that possess both Lewis and Brønsted acidity and have been applied as selective catalysts in various reactions.[5−8] Although the acidity of these samples has been suggested to be due to the distortion of the Si−O−Si lattice structure,[6,8] the detailed mechanism is still unclear. Acidic silica materials are important key materials not only for synthetic chemistry but also for basic catalytic science. The development of novel acidic silica materials is an important subject in materials science. However, to date, the preparation of mesoporous silica with excellent catalytic properties still involves multistep synthetic routes, such as aging and hydrothermal processes from silica sources using surfactants and then subsequent firing processes.[2−8] Here we propose a one-step synthetic route for the production of acidic silica using a natural iron oxide of bacterial origin as the starting material. In recent years, another notable study on mesoporous silica using a biomimetic approach was reported and attracted many researchers' attention.[9]

Recently, we reported that "biogenous iron oxides (BIOXs)", products of iron-oxidizing bacteria,[10,11] contains large amounts of silicon, in addition to iron.[12−16] Although BIOXs have been regarded as unwanted materials, we focused on the development of practical applications using these novel functional materials[12−14] from a materials science perspective. The target BIOX in this study is iron oxide microtubules (*L*-BIOX) produced by *Leptothrix ochracea*. *L*-BIOX is primarily composed of an amorphous iron oxide (Fe:Si:P = 73:22:5 in an atomic ratio, with the exception of oxygen, hydrogen, and carbon) nanoparticles with a diameter of ~3 nm.[15] The primary nanoparticles are aggregated to form secondary particles that are several tens of nanometers in size,[13,16] and finally these particles are intricately interconnected into microtubules that are ~1 μm in diameter.[13,16]

The silicon in *L*-BIOX seems to be an attractive silica source. Herein, we describe the one-step preparation of acidic silica from natural *L*-BIOX. The basic characteristics of the biogenous silica material, such as its morphological, compositional, and porous features and its acidic properties, including its catalytic performance, are reported. In addition, the catalytic

Received: May 7, 2012
Accepted: January 18, 2013
Published: January 18, 2013

properties of the biogenous silica material are compared with those of conventional silica catalysts.

EXPERIMENTAL SECTION

Sample Preparation and Characterization. *L*-BIOX was obtained as an ocher precipitate from a water-purifying tank.[12] It was washed repeatedly with distilled water[12] and dried in air at room temperature. To dissolve the iron content from *L*-BIOX, the dried powder was immersed in a 35 wt % hydrochloric acid solution with stirring for 3 days. The resulting precipitate was filtered, washed with distilled water, and then vacuum-dried. The sample was characterized using several analytical methods. The crystallographic and morphological features were examined by X-ray diffractometry (XRD; RINT-2000; Rigaku, Japan), scanning electron microscopy (SEM; S-4300; Hitachi, Japan), and transmission electron microscopy (TEM; JEM-2100F; JEOL, Japan). Elemental analysis was performed using inductively coupled plasma mass spectroscopy (ICP-MS; ELAN DRC-II; PerkinElmer, Japan). The surface area and micro- and mesopore-size distributions were obtained from nitrogen adsorption isotherms at 77 K (BELSORP-mini-II; BEL Japan) using the Brunauer–Emmett–Teller (BET) method,[17] the micropore analysis (MP) method,[18] and the Dollimore–Heal (DH) method,[19,20] respectively. The glass transition temperature (T_g) was determined by differential thermal analysis (DTA; SDT Q600; TA Instruments, Japan) measurements. An upscan to 1563 K and a downscan were performed at 20 K/min at an air flow of 100 mL/min. Subsequent accumulated second to tenth upscan and downscan with 20 K/min at 973–1563 K were used to determine T_g. The state of iron in the sample was characterized by diffuse-reflectance ultraviolet–visible–near-IR (DR UV–vis–NIR) spectroscopy. The spectrum was measured at room temperature using a JASCO V-570 UV–vis–NIR spectrophotometer (JASCO Co., Japan) equipped with an integral sphere. The pretreatment of the sample was carried out by evacuation at room temperature for 2 h under a reduced pressure of 1.3 mPa.

Evaluation of Acidic Centers. Because IR spectroscopy of adsorbed probe molecules is commonly employed as a useful technique for clarifying the state of the solid surface,[21,22] the solid acid properties were investigated by Fourier transform infrared (FTIR) spectroscopy. FTIR spectra were recorded at room temperature on a Digilab FTS4000MXK FTIR spectrophotometer (Randolph, USA) with a mercury–cadmium–telluride (MCT) detector maintained at liquid-N_2 temperature. A total of 144 detector readings were accumulated at a spectral resolution of 2 cm^{-1}. The sample (~8 mg) was pressed into a 10-mm pellet and placed in a quartz cell with KRS-5 windows. This cell enables sample pretreatment and the subsequent introduction of gas in situ.[23] Sample pretreatment was performed by evacuation at room temperature for 2 h under a reduced pressure of 1.3 mPa, followed by exposure to pyridine (Py; 99.8% purity; Sigma-Aldrich) at a pressure of ~26 Pa at room temperature. After adsorption, the sample was evacuated at a definite temperature for 1 h under a reduced pressure of 1.3 mPa. The intensity of the band was corrected by normalizing the intensity of the skeletal mode of samples at around 2000 cm^{-1}. Unprocessed *L*-BIOX, a synthetic acidic silica, MCM-41,[6] and a commercially available nearly neutral silica (Aerosil200; Nippon Aerosil Co., Ltd.) were also measured as reference samples. MCM-41 containing a slight amount of iron (Si/Fe = 155), MCM-41-Fe, was synthesized for a reference sample. MCM-41, synthesized referring to ref 6, was dispersed in an aqueous solution of $Fe(NO_3)_3$ with stirring for 6 h at room temperature. The obtained sample was centrifuged, washed with distilled water, dried at 353 K, and finally heat-treated at 773 K for 6 h in air.

General Procedure for the Catalytic Reactions. The catalytic activity of the silica sample, *L*-BIOX, MCM-41, and Aerosil200 was evaluated for the ring-opening reaction of styrene oxide (Scheme 1a) and the Friedel–Crafts reaction of indole with methyl vinyl ketone (Scheme 1b). These reactions were conducted under ordinary conditions, and the reaction products were characterized by ^1H NMR (Varian 600 VNMRS) and analytical thin-layer chromatography (TLC). A spent silica sample was filtered through a 0.2-μm-membrane filter, washed with ethyl acetate and methanol, dried under vacuum, and then characterized by XRD, ICP-MS, nitrogen adsorption method, and IR spectroscopy. We also conducted reuse experiments of the spent silica sample.

Scheme 1. (a) Ring-Opening Reaction of an Epoxide and (b) Friedel–Crafts-Type Alkylation

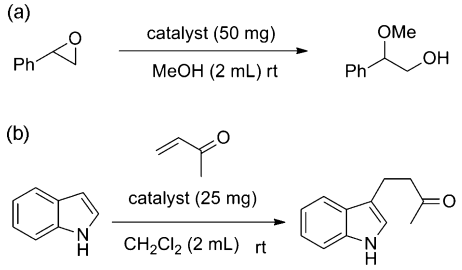

Ring-Opening Reaction of Styrene Oxide. First, to a solution of styrene oxide (0.12 mL, 1 mmol) in methanol (2 mL) was added a catalyst (50 mg) at 300 K, and the suspension was stirred until the reaction was complete as determined by TLC. The methanol was then removed using a rotary evaporator. The resultant residue was purified by column chromatography to give a colorless oil. ^1H NMR (600 MHz, NMR): δ 3.14 (s, 3H), 3.53 (dd, 1H, J = 3.7 and 11.7 Hz), 3.59 (dd, 1H, J = 8.6 and 11.7 Hz), 4.22 (dd, 1H, J = 3.7 and 8.6 Hz), 7.2–7.4 (m, 5H).

Friedel–Crafts Reaction of Indole with Methyl Vinyl Ketone. First, to a solution of indole (50 mg, 0.427 mmol) in CH_2Cl_2 (2 mL) was added methyl vinyl ketone (0.1 mL, 1.23 mmol). Second, the catalyst (25 mg) was added to this solution at 300 K. Third, the suspension was stirred until the reaction was complete as determined by TLC. Next, the suspension was purified by column chromatography to give a white solid. ^1H NMR (600 MHz, $CDCl_3$): δ 2.07 (s, 3H), 2.78 (t, 2H, J = 7.6 Hz), 2.85 (t, 2H, J = 7.6 Hz), 6.92 (s, 1H), 7.0–7.6 (m, 4H), 7.88 (b, 1H).

RESULTS AND DISCUSSION

Figure 1 shows the XRD patterns and photographs of *L*-BIOX and the acid-leached sample. *L*-BIOX had an ocher color, while

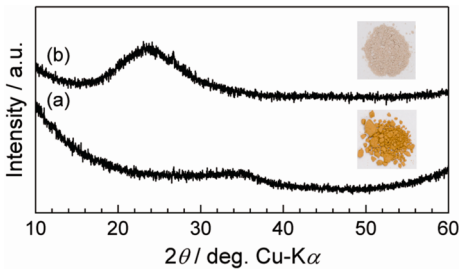

Figure 1. XRD patterns of (a) *L*-BIOX and (b) the acid-leached sample. Inset images are photographs of the respective samples.

the acid-leached sample was gray. A broad XRD peak appearing at the *d*-spacing value of 0.39 nm was compatible with the formation of amorphous silica in the acid-leached sample. The Si/Fe and Si/P ratios measured by ICP-MS were ~150 and ~6600, respectively. Nearly all of the iron and phosphorus ions were dissolved. The sample was strongly aggregated with granular primary particles of 6.1 ± 1.9 nm diameter (dotted circle in Figure 2c) and did not maintain the tubular shape of *L*-BIOX (Figure 2). Although there are no distinctive pores in the primary particles, many pores of 2.4 ± 1.9 nm diameter were observed at the interspace of the primary particles (Figure 2c, arrows). The BET surface area calculated from the nitrogen

dx.doi.org/10.1021/am302837p | ACS Appl. Mater. Interfaces 2013, 5, 518–523

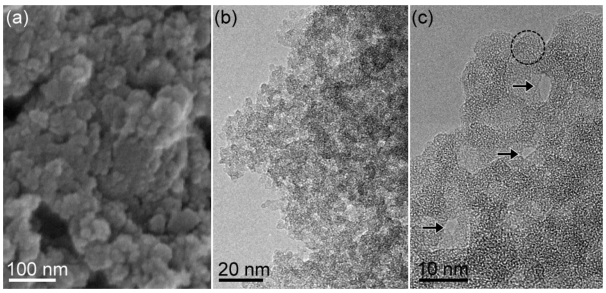

Figure 2. (a) SEM, (b) TEM, and (c) high-magnification TEM images of the acid-leached sample. The dotted circle and arrows show the primary particle and fine pores, respectively.

adsorption isotherms for the sample had a very large value (540 m^2/g), which is twice as large as that of the original *L*-BIOX (280 m^2/g).[13] The pore-size distribution calculated by the DH and MP methods revealed that the sample is a porous material having micropores with d_p = 1.4 nm (Figure 3a) and a small

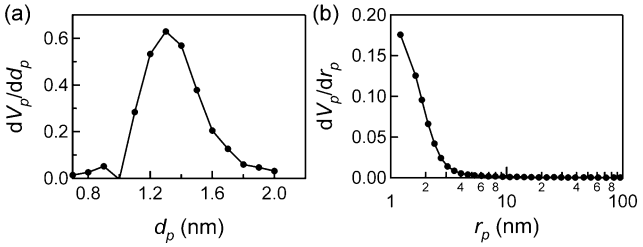

Figure 3. Pore-size distributions of (a) micropores and (b) mesopores as calculated by the MP and DH methods, respectively.

amount of mesopores with r_p < 3 nm (Figure 3b). Some of such micropores and mesopores could form at interspaces of aggregated primary particles, as observed in TEM image (Figure 2c, arrows). The chemical formula with structural OH groups excluding physisorbed water was calculated to be $SiO_2 \cdot 0.4H_2O$ based on the weight change after heating at 1273 K for 2 h, as determined by thermogravimetry. We considered the weight losses below and above 403 K to be attributed to dehydration of physisorbed water and structural OH groups, respectively. According to DTA, the broad endotherm that must be associated with the glass transition of silica was observed near 1400 K. This suggests that the sample is amorphous, which is consistent with the above XRD results. The T_g value of the sample was found to be near 1410 K, which is ~70 K lower than that of pure silica glass.[24] This lower T_g could be due to the incorporation of hydroxyl groups in the glass structure and/or the very small amount of iron in the sample. The further investigation concerning the glassy nature and relationship of T_g and the microstructure of the present sample will be discussed in our future work.

The mechanism of formation for the sample was speculated to be as follows. *L*-BIOX is composed of amorphous iron oxide containing structural silicon and phosphorus (Fe:Si:P = 73:22:5 in atomic ratio), and all of the elements are distributed uniformly.[12,16] When *L*-BIOX was immersed in a strong acid solution, all of the elements dissolved and existed in an ionic state: ferric, silicate, and phosphate ions. Polymerization of silicate ions occurred immediately in a strong acid solution, and amorphous silica was reprecipitated. The original tubular form of *L*-BIOX was considered to be broken in the first dissolved step. This idea is quite reasonable in terms of the structural model of pristine *L*-BIOX. We proposed the amorphous structure model of *L*-BIOX in our previous study.[15] In this model, silicon atoms exist as isolated SiO_4 monomers or Si_2O_7 dimers in the framework network of FeO_6 octahedral units and there are no silica networks. According to this structural model, when the FeO_6 network is dissolved by an acid solution, silicon atoms are definitely dissolved as SiO_4 monomers or Si_2O_7 dimers. Therefore, solid silica could form a subsequent precipitation process. Here we refer to the acid-leached sample as "biogenous silica (BSL)".

Further characterization of BSL was performed by DR UV−vis−NIR and IR spectroscopies by comparison with reference samples. The DR UV−vis−NIR spectrum of BSL treated at 300 K exhibits absorption bands at around 46000, 40000, 30000, 25000, and 17000 cm^{-1} (arrows in Figure 4a). The former two bands are ascribed to the transitions with ligand-to-metal (i.e., Fe^{3+}) charge-transfer character, and the band at 30000 cm^{-1} is due to the octahedral Fe^{3+} species.[25,26] The weak bands at 25000 and 17000 cm^{-1} are assigned to the d−d transitions of Fe^{3+} in tetrahedral symmetry. In addition to these bands, the intense bands at around 20000 and 13000 cm^{-1} (arrowheads in Figure 4a), which are due to the Fe_2O_3 species,[26] appear in the case of *L*-BIOX. Although the quantitative discussion is difficult from the present DR UV−vis−NIR data, these results indicate that the acid-leaching treatment apparently removes iron oxide species. In the IR spectrum of a 300 K treated BSL sample, the broad bands are observed at 3300 and 1630 cm^{-1} (arrows in Figure 4b). These bands are assigned to O−H stretching and bending vibrations, respectively.[27,28] In addition, the characteristic bands at around 3741, 3695, and 3622 cm^{-1} clearly appear (arrows in the inset of Figure 4b), which are due to the O−H stretching modes of OH groups attached to silicon,[29−32] iron,[33] and iron and silicon,[34] respectively, indicating that the surface of BSL consists of linkages of the Si−OH, Fe−OH, and Si−OH−Fe.

The solid acid properties of BSL were examined by IR using Py as the probe molecule. Parts b and c of Figure 4 show the IR spectra for BSL treated under various conditions (1−7), *L*-BIOX (the starting material, A), MCM-41 (acidic silica, B), and Aerosil200 (neutral silica, C). When the samples were exposed to Py vapor at room temperature, some absorption bands appeared (Figure 4c, 2, A−C). The very weak bands at ~1600, ~1450, and ~1490 cm^{-1} for Aerosil200 were assigned to hydrogen-bonded Py species,[35] indicating that Aerosil200 is nearly neutral. Such bands almost disappeared by reevacuation at low temperature (i.e., weak interaction). In contrast, the strong bands at ~1600 and ~1450 cm^{-1} assigned to the Py species adsorbed on Lewis acid sites[36−38] and the band at ~1480 cm^{-1} assigned to the Py species adsorbed on both Lewis and Brønsted acid sites[36−38] (i.e., strong interaction) were observed in all other samples. The weak bands observed at 1640 and 1548 cm^{-1} for BSL, *L*-BIOX, and MCM-41 (Figure 4c, 2, and A and B) typically appear when Py is adsorbed on Brønsted acid sites (i.e., a hydroxyl group bridging silicon and aluminum atoms in the framework Si···(OH)···Al in the case of zeolite).[36−38] These above results indicate that relatively strong Lewis and Brønsted acid sites exist in BSL, *L*-BIOX, and MCM-41.

The spectrum profile of BSL is different from that of *L*-BIOX and analogous to that of MCM-41, indicating that BSL has acidic sites analogous to those of MCM-41. The intensity of the bands assigned to Lewis acid sites (~1600 and ~1450 cm^{-1}) is

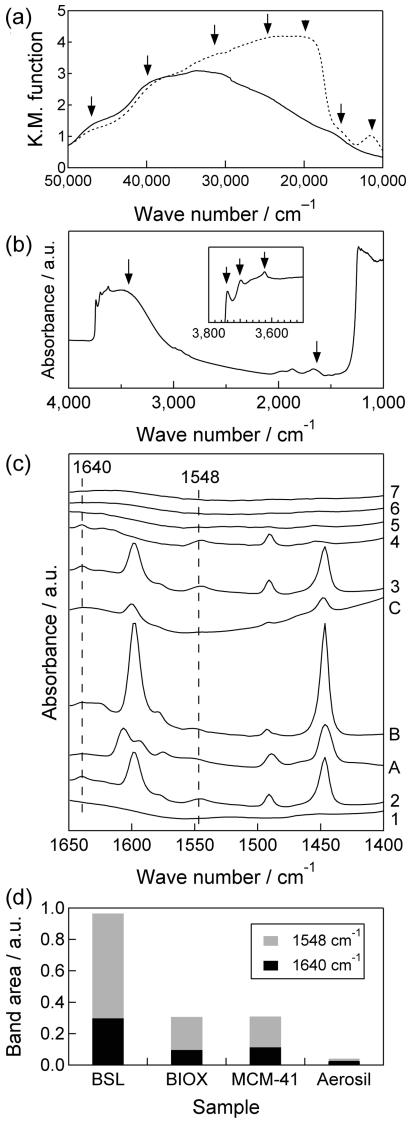

Figure 4. (a) DR UV−vis−NIR spectra of BSL (solid line) and *L*-BIOX (dotted line) treated at 300 K. (b) IR spectrum of BSL evacuated at 300 K. (c) IR spectra of BSL treated under various conditions: (1) evacuation at 300 K; (2) exposure to Py vapor at approximately 26 Pa at room temperature; (3−7) reevacuation at 300, 373, 473, 573, and 673 K, respectively. (A−C) Spectra for *L*-BIOX, MCM-41, and Aerosil200 exposed to Py under the same conditions as those for BSL, respectively. (d) Areas of the bands at 1640 and 1548 cm^{-1} obtained from the IR spectra versus the samples.

largest for MCM-41, but the intensity of the bands assigned to Brønsted acid sites (~1640 and 1548 cm^{-1}) seems to be the largest for BSL. The area of bands at 1640 and 1548 cm^{-1} were compared for each sample (Figure 4d). The band area for BSL is larger than those for *L*-BIOX and MCM-41, indicating that the amount of Brønsted acid sites in BSL is the greatest among the measured samples in this study. In addition, the Py species adsorbed on BSL desorbed completely through evacuation at temperatures around 573−673 K (Figure 4c, 3−7). The desorption temperature of the Py species on the BSL was slightly higher than those for MCM-41 (473−573 K) and *L*-BIOX (473−573 K), indicating that hydroxyl groups with a relatively strong acidic nature exist in the BSL. Therefore, an acidic silica material with a Lewis acid nature and a relatively strong Brønsted acid nature was successfully obtained from the natural iron oxide.

The BSL contains slight amounts of iron (Si/Fe = ~150), and these iron ions could act like aluminum in zeolites [i.e., Si···(OH)···Fe], causing the BSL to be Brønsted acidic. More recently, nearly pure silica samples (Si/Fe > 1000) were prepared from *L*-BIOX using a different acid, high-temperature concentrated nitric acid. Although these silica samples scarcely contain iron ions in comparison with the BSL, their surfaces exhibit similar acidic properties; therefore, the origin of the specific acidic nature of the silica is most likely similar to that of the FSM-16 and MCM-41 samples. This result might suggest that the generation of acid sites in the BSL is caused by not only the existence of hydroxyl groups arising from the Si···(OH)···Fe structure[36−38] but also the distortion of the Si−O−Si lattice structure,[6,8] although these details remain unclear. On the other hand, the appearance of the Lewis acid sites is considered to be due to the small amount of iron existing on BSL.

The BSL sample investigated in this study was then applied as a catalyst for two representative acid-catalyzed organic reactions (the ring opening of an epoxide and a Friedel−Crafts-type alkylation; Scheme 1). *L*-BIOX and the two well-known silica samples, MCM-41 and Aerosil200, were also examined to evaluate the catalytic activity of the BSL. In these reactions, the Brønsted acid sites of the catalyst activate the epoxide (Scheme 1a) and the carbonyl functional group of methyl vinyl ketone (Scheme 1b). All reactions were monitored by TLC analysis at appropriate time intervals, and all reactions were stopped at the time to reach reaction equilibrium (except the reaction using Aerosil200). In the epoxide ring-opening reaction (Table 1, reaction a), the BSL, *L*-BIOX, and MCM-41 effectively catalyzed the reaction to give products in good yields (BSL, 78%; *L*-BIOX, 71%; MCM-41, 70%), while Aerosil200 gave a poor yield (<2%). Similar results were obtained in the Friedel−Crafts-type alkylation reaction (Table 1, reaction b), although the yield for *L*-BIOX (46%) was less than those of BSL (84%) and MCM-41 (74%). In order to compare the catalytic activity of BSL and MCM-41, we conducted the catalytic reaction using BSL for the same reaction time as MCM-41 (in reaction a, 2.5 h, and in reaction b, 3 days). BSL gave the product in moderate yields (47% in reaction a and 40% in reaction b), indicating that the BSL catalyst has about half the catalytic activity of MCM-41. We synthesized MCM-41 with nearly the same amount of Fe^{3+} for BSL (MCM-41-Fe; Si/Fe = 155) and also examined its catalytic activity to confirm the effect of Fe^{3+} in BSL for its catalytic activity. The yield of both reactions using MCM-41-Fe as a catalyst did not show a simple increment. MCM-41-Fe gave a low yield (15%) in reaction a and a good yield (82%) in reaction b. Although the reason why the low yield in reaction a is now unclear, these results suggest that Fe^{3+} in BSL could not

Table 1. Reaction Yields Using Different Silica Samples as the Catalyst

	reaction a		reaction b	
catalyst	yield/%	time	yield/%	time/days
BSL	78	33 h	84	5
L-BIOX	71	7 days	46	7
Aerosil200	<2	48 h	5	5
MCM-41	70	2.5 h	74	3
BSL	47	2.5 h	40	3

dx.doi.org/10.1021/am302837p | *ACS Appl. Mater. Interfaces* 2013, 5, 518−523

be an essential component for the catalytic activity of BSL. All of these results support the idea that the BSL has relatively strong Brønsted acid sites and that it works as an active acid catalyst for organic reactions.

We recovered BSL after reactions a and b and characterized its properties. The properties concerning amorphous structure, iron content, particle sizes, and surface area were not changed. However, according to IR spectroscopy, the intensity of the band at 1640 and 1548 cm^{-1} (Brønsted acid sites) weakens after reaction because of the surface adsorption of organic species. Also, we conducted reuse experiments of recovered BSL (Table 2). The catalytic activity was significantly reduced

Table 2. Catalytic Performance of the Recovered BSL Catalyst in Reactions a and b

	reaction a		reaction b	
run	yield/%	time/h	yield/%	time/days
1	78	33	84	5
2	42	33	53	5
3	24	33	57	5

in reaction a from 78% in the first run to 24% in the third run; on the other hand, the yield of reaction b in the third run retained ~70% of that in the first run. These results suggest that the BSL catalyst requires some kinds of activation procedures prior to reuse, and efforts are underway in our group.

Separately, the same acid-leaching experiment was carried out with BIOX samples produced by *L. ochracea* and *Gallionella ferruginea* from another sampling site at Okayama University.[16,39] Regardless of the different sampling sites and bacterial species, amorphous silica with nearly the same acid properties as those for the BSL in this study was obtained. These results indicate that any silicon-containing BIOX can be transformed into acidic amorphous silica. The details of these two samples will be published elsewhere.

CONCLUSIONS

Acidic amorphous silica was synthesized by a novel synthetic route: iron oxide produced by iron-oxidizing bacteria was dissolved in a concentrated hydrochloric acid solution, and the resulting product was dried. This new silica material has strong acid sites and a high surface area with distinctive micro- and mesopores and works as an acid catalyst for the ring-opening reaction of epoxides and Friedel–Crafts-type alkylations: BSL is very active for acid-catalyzed reactions, like the mesoporous silica MCM-41 and in contrast to the nonporous silica Aerosil200, but it has a pore-size distribution very different from that of MCM, in the upper range of microporosity.

AUTHOR INFORMATION

Corresponding Author

*E-mail: jtakada@cc.okayama-u.ac.jp.

Author Contributions

The manuscript was written through contributions of all authors. All authors have given approval to the final version of the manuscript.

Notes

The authors declare no competing financial interest.

ACKNOWLEDGMENTS

The authors thank K. Yamashita, Y. Yamano, Y. Kishimoto, and M. Nakamura for helpful discussions. This study was financially supported by a Special Grant for Education and Research from the Ministry of Education, Culture, Sports, Science, and Technology, Japan (to J.T.), and JSPS KAKENHI Grants 22860040, 24760550, and 23360309.

REFERENCES

(1) Wang, W.; Hunger, M. *Acc. Chem. Res.* **2008**, *41*, 895–904.
(2) Kresge, C. T.; Leonowicz, M. E.; Roth, W. J.; Vartuli, J. C.; Beck, J. S. *Nature* **1992**, *359*, 710–712.
(3) Corma, A. *Chem. Rev.* **1997**, *97*, 2373–2419.
(4) Thomas, J. M. *Angew. Chem., Int. Ed.* **1999**, *38*, 3588–3628.
(5) Ishitani, H.; Iwamoto, M. *Tetrahedron Lett.* **2003**, *44*, 299–301.
(6) Iwamoto, M.; Tanaka, Y.; Sawamura, N.; Namba, S. *J. Am. Chem. Soc.* **2003**, *125*, 13032–13033.
(7) Haishi, T.; Kasai, K.; Iwamoto, M. *Chem. Lett.* **2011**, *40*, 614–616.
(8) Yamamoto, T.; Tanaka, T.; Funabiki, T.; Yoshida, S. *J. Phys. Chem. B* **1998**, *102*, 5830–5839.
(9) Jensen, M.; Keding, R.; Höche, T.; Yue, Y. *J. Am. Chem. Soc.* **2009**, *131*, 2717–2721.
(10) Ghiorse, W. C. *Annu. Rev. Microbiol.* **1984**, *38*, 515–550.
(11) Emerson, D.; Fleming, E. J.; McBeth, J. M. *Annu. Rev. Microbiol.* **2010**, *64*, 561–583.
(12) Hashimoto, H.; Yokoyama, S.; Asaoka, H.; Kusano, Y.; Ikeda, Y.; Seno, M.; Takada, J.; Fujii, T.; Nakanishi, M.; Murakami, R. *J. Magn. Magn. Mater.* **2007**, *310*, 2405–2407.
(13) Ema, T.; Miyazaki, Y.; Kozuki, I.; Sakai, T.; Hashimoto, H.; Takada, J. *Green Chem.* **2011**, *13*, 3187–3195.
(14) Mandai, K.; Korenaga, T.; Ema, T.; Sakai, T.; Furutani, M.; Hashimoto, H.; Takada, J. *Tetrahedron Lett.* **2012**, *53*, 329–332.
(15) Hashimoto, H.; Fujii, T.; Kohara, S.; Asaoka, H.; Kusano, Y.; Ikeda, Y.; Nakanishi, M.; Benino, Y.; Nanba, T.; Takada, J. *Mater. Chem. Phys.* **2012**, *137*, 571–575.
(16) Suzuki, T.; Hashimoto, H.; Ishihara, H.; Kasai, T.; Kunoh, H.; Takada, J. *Appl. Environ. Microbiol.* **2011**, *77*, 7873–7875.
(17) Brunauer, S.; Emmett, P. H.; Teller, E. *J. Am. Chem. Soc.* **1938**, *60*, 309–319.
(18) Mikhail, R. S.; Brunauer, S.; Bodor, E. *J. Colloid Interface Sci.* **1968**, *26*, 45–53.
(19) Dollimore, D.; Heal, G. *J. Appl. Chem.* **1964**, *14*, 109–114.
(20) Dollimore, D.; Heal, G. *J. Colloid Interface Sci.* **1970**, *33*, 508–519.
(21) Davydov, A. A. *Infrared spectroscopy of adsorbed species on the surface of transition metal oxides*; John Wiley & Sons Inc.: New York, 1984.
(22) Lamberti, C.; Zecchina, A.; Groppo, E.; Bordiga, S. *Chem. Soc. Rev.* **2010**, *39*, 4951–5001.
(23) Kuroda, Y.; Maeda, H.; Morimoto, T. *Rev. Sci. Instrum.* **1989**, *60*, 3083–3085.
(24) Richet, P. *Geochim. Cosmochim. Acta* **1984**, *48*, 471–483.
(25) Inui, T.; Nagata, H.; Takeguchi, T.; Iwamoto, S.; Matsuda, H.; Inoue, M. *J. Catal.* **1993**, *139*, 482–489.
(26) Bordiga, S.; Buzzoni, R.; Geobaldo, F.; Lamberti, C.; Giamello, E.; Zecchina, A.; Leofanti, G.; Petrini, G.; Tozzola, G.; Vlaic, G. *J. Catal.* **1996**, *158*, 486–501.
(27) Nakamoto, K. *Infrared and Raman spectra of inorganic and coordination compounds*, 5th ed.; John Wiley & Sons, Inc.: NewYork, 1997; pp 88–95.
(28) Jitianu, A.; Crisan, M.; Meghea, A.; Rau, I.; Maria, Z. *J. Mater. Chem.* **2002**, *12*, 1401–1407.
(29) Vansant, E. F.; Van Der Voort, P.; Vrancken, K. C. *Stud. Surf. Sci. Catal.* **1995**, *93*, 59–77.
(30) Zecchina, A.; Bordiga, S.; Spoto, G.; Marchese, L. *J. Phys. Chem.* **1992**, *96*, 4985–4990.

(31) Zecchina, A.; Bordiga, S.; Spoto, G.; Marchese, L. *J. Phys. Chem.* **1992**, *96*, 4991−4997.
(32) Seehra, M. S.; Roy, P.; Raman, A.; Manivannan, A. *Solid State Commun.* **2004**, *130*, 597−601.
(33) Ishikawa, T.; Saito, H.; Yasukawa, A.; Kandori, K. *Bull. Chem. Soc. Jpn.* **1996**, *69*, 899−907.
(34) Berlier, G.; Spoto, G.; Bordiga, S.; Ricchiardi, G.; Fisicaro, P.; Zecchina, A.; Rossetti, I.; Selli, E.; Forni, L.; Giamello, E.; Lamberti, C. *J. Catal.* **2002**, *208*, 64−82.
(35) Zaki, M. I.; Hasan, M. A.; Al-Sagheer, F. A.; Pasupulety, L. *Langmuir* **2000**, *16*, 430−436.
(36) Parry, E. P. *J. Catal.* **1963**, *2*, 371−379.
(37) Parker, L. M.; Bibby, D. M.; Burns, G. R. *J. Chem. Soc., Faraday Trans.* **1991**, *87*, 3319−3323.
(38) Buzzoni, R.; Bordiga, S.; Ricchiardi, G.; Lamberti, C.; Zecchina, A. *Langmuir* **1996**, *12*, 930−940.
(39) Suzuki, T.; Hashimoto, H.; Matsumoto, N.; Furutani, M.; Kunoh, H.; Takada, J. *Appl. Environ. Microbiol.* **2011**, *77*, 2877−2881.